Break-Off of an Air Bubble within a Thin Oil Layer

Honors Undergraduate Thesis by

Brooks Campbell

The University of Texas at Austin

Department of Physics

Center for Nonlinear Dynamics

May 2007

Acknowledgements

Funding for this work was provided by a Schlumberger Undergraduate Research Fellowship.

I would like to thank Harry Swinney for providing invaluable guidance throughout this project. He has made this project the high point of my undergraduate education, and it has been an honor to work with such an accomplished physicist.

I thank Matthew Thrasher for helping me in the lab on a daily basis. He has taught me the ins and outs of the entire experimental process showing great insight and expertise. On many, many occasions he stopped his own work, even in the midst of his dissertation, to help me whenever I asked. I couldn't have asked for a more helpful and friendly mentor.

I would like to thank Mark Mineev for providing helpful discussions of the theoretical aspects of this project.

I also thank my parents, Aaron and Michele, brother, Hunter, and grandparents, Dom, Bop, Glen, and Viv, for all of their love, support, and prayers throughout this project and my entire college career.

Table of Contents

Abstract

We examine the process of bubble break-off in a fluid confined between two closely spaced parallel plates (called a Hele-Shaw cell) to test a theorized connection between this process and a well studied body of mathematics. Bubble break-off here is the process with a bubble of a less viscous fluid surrounded by a more viscous fluid breaking apart into two bubbles. In our case an annulus of air surrounded by silicone oil undergoes a break-off event to become a simply connected domain of air. The Hele-Shaw cell confines the fluid to quasi-two-dimensional flows. Lee *et al.* have provided a theory detailing the time evolution of a bubble interface undergoing a break-off event in a region near the point of break-off. We collected high-resolution images of bubbles breaking off at 200 to 1000 frames per second and compared the experimental interface to the theoretical one. We found that the theory was accurate for a region about 50 b (where b is the thickness of the oil layer) for times before break-off. Initial data analysis does not indicate any time scaling law associated with our bubble break-off, which contradicts theory. At this time we are currently working with the theory and data to find stronger results indicating or disproving a connection between the two. Further analysis must be done to determine if our experimental conditions match those required by the theory since the suggested experimental conditions in Lee's idealized situation are difficult to realize in a physical system.

Introduction

1.1 Bubble Break-off in Hele-Shaw cells

Quasi two-dimensional fluid flows have become an important division of fluid dynamics. These flows are directly relevant to recovering oil from reservoirs because of their mathematical equivalence to flows in porous media.

Hele-Shaw cells, which consist of a narrow gap between two plates, provide a viable way to study fluids in a quasi two-dimensional setting. In our case one of these plates has one or two inlets that I use to inject fluids into the gap. When two immiscible fluids, such as air and silicone oil, are injected into the cell, a sharp interface forms between them. These cells are useful experimental tools because they allow fluid interactions to be easily imaged without the use of dyes or other involved imaging techniques—a luxury rarely experienced in fluid research.

The purpose of this paper is to test a theorized connection between an extensive body of well-established mathematics and bubble break-off in a Hele-Shaw cell. Bubble break-off is the term for what happens when a single bubble of fluid separates into two bubbles. More generally break-off occurs when a multiply connected domain reduces the number of connections by one. In particular I examine the case in which an annulus of air undergoes a single break-off event and becomes a simply connected bubble. By manipulating pumping rates of the fluids and which fluid is pumped, I arrange for air bubble break-off to occur and take high-resolution photos of the event.

Lee *et al*. have provided a theory that describes bubble break-off in an idealized system, a purely two-dimensional geometry where the interface between the fluids has zero surface tension [1]. The result is a set of functions that predict the time evolution of a bubble interface near the region of break-off both before and after the event. They show that the solution is a dispersionless limit of the ANKS hierarchy (dANKS), a well-established body of mathematics dealing with nonlinear dynamics, solitons, and integrable systems which makes connections to quantum, optical, and hydrodynamic physics. Experimental confirmation of this theory could lead to further extensions of the dANKS hierarchy and a better understanding of Hele-Shaw flows and phenomena.

Background

2.1 Hele-Shaw Cells

When a second liquid is injected into a Hele-Shaw cell, the two immiscible fluids will form a sharp interface that can be manipulated by pumping the fluids in or out. Hele-Shaw cells provide a particularly nice experimental setup because they are generally made of two transparent plates, glass or Plexiglas in our case, which allow for convenient imaging of the fluid interfaces.

Hele-Shaw cells are named as such because they were built in accordance with the experimental conditions described in a theoretical paper written by H.S. Hele-Shaw in 1898 [2]. Most theories of Hele-Shaw flows model the system in a purely two-dimensional manner so the gap is usually very narrow.

In this paper we conduct experiments in two different Hele-Shaw cells. First a radial cell which is made of two circular plates of glass with a single inlet in the center; the second cell is rectangular and has two inlets along one of the diagonals of the plates (Fig. 1). In addition to its experimental convenience, fluid movement in a Hele-Shaw cell is a practical topic to study because they are mathematically equivalent to flows in porous material, e.g. the flow of oil when

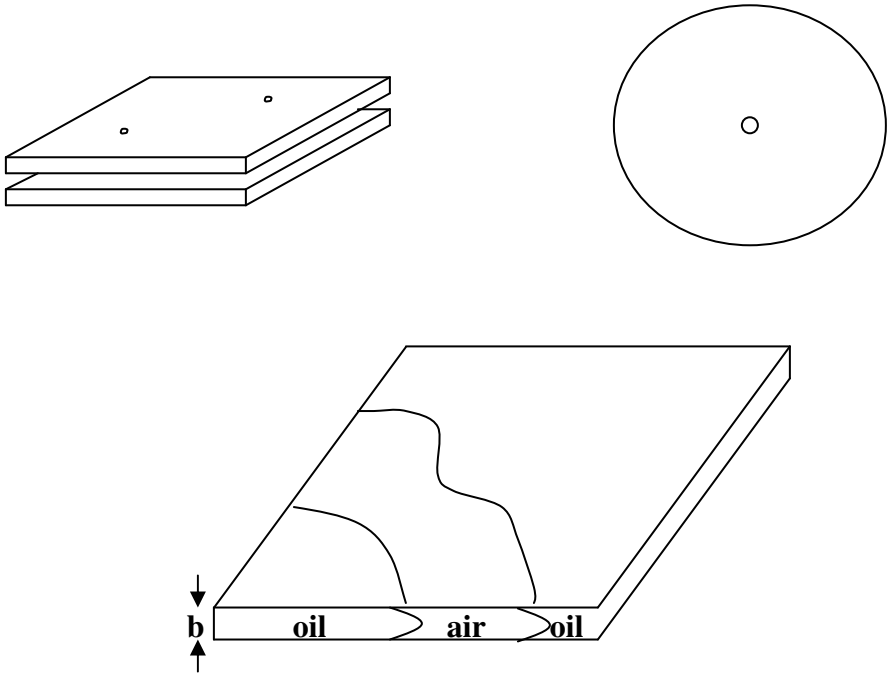

Figure 1: Top Left: Side View of a rectangular Hele-Shaw cell with two inlets in the top plate. Top Right: Top view of a circular Hele-Shaw cell with a single inlet in the center. Bottom: A sample interface between an air bubble surrounded by silicone oil inside of a Hele-Shaw cell.

it is extracted from reservoirs of porous sand or rock [2]. For a description of these cells including their exact dimensions please see the Methods section 3.1.

2.2 Hele-Shaw flows

Hele-Shaw flows were first examined in 1898. In Hele-Shaw's original paper he derived equations of motion for these quasi two-dimensional flows. Below is a derivation describing flows in a Hele-Shaw cell, which is an assumption made in Lee's derivation of the self-similar result.

Begin with the Navier-Stokes equation where $\underline{v}$ is the velocity vector, ρ is density, and υ is the dynamic viscosity as noted in Fig. 2 [3].

$$\frac{d\underline{v}}{dt} + (\underline{v}\cdot\nabla)\underline{v} = -\frac{\nabla p}{\rho} + \upsilon\nabla^2\underline{v} \qquad (1)$$

The two terms on the left side of the equation can be neglected under the following assumptions. The $d\underline{v}/dt$ term can be neglected if we assume steady flow, and $(\underline{v}\cdot\nabla)\underline{v}$ can be neglected if we assume $\underline{v}$ is small so that $\underline{v}^2$ is higher order and negligible. Under these assumptions we conclude the following.

$$-\frac{\nabla p}{\rho} + \upsilon\nabla^2\underline{v} = 0 \qquad (2)$$

Then by multiplying by ρ we convert the kinematic viscosity, υ, to the dynamic viscosity, μ since $\upsilon\rho=\mu$. I assume that the fluids are incompressible so the density, ρ, is constant. Then by moving the first term to the other side and separating the vector equation into three equations we get equations 3-5.

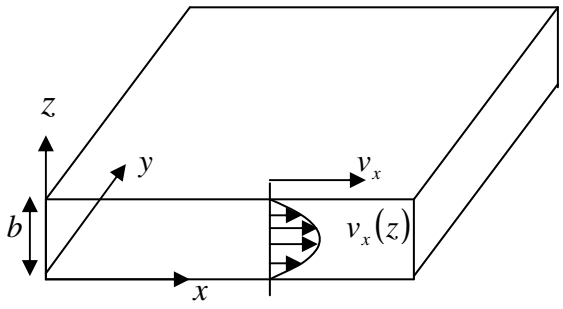

Figure 2: We examine the case of fluid flow between two plates when only a single fluid is present. The gap thickness, b, velocity profile, $v_x(z)$, and the coordinate system used in the derivation below are defined here.

$$\frac{dp_x}{dx} = \mu\left(\frac{d^2v_x}{dx^2} + \frac{d^2v_x}{dy^2} + \frac{d^2v_x}{dz^2}\right) \quad (3)$$

$$\frac{dp_y}{dy} = \mu\left(\frac{d^2v_y}{dx^2} + \frac{d^2v_y}{dy^2} + \frac{d^2v_y}{dz^2}\right) \quad (4)$$

$$\frac{dp_z}{dz} = \mu\left(\frac{d^2v_z}{dx^2} + \frac{d^2v_z}{dy^2} + \frac{d^2v_z}{dz^2}\right) \quad (5)$$

Now we assume that the pressure gradient is only non-zero in the x direction and that the velocity is only in the direction of the pressure gradient. Therefore the left and right sides of equations (4) and (5) are zero. Then in equation (3), $\frac{d^2v_x}{dy^2}$ and $\frac{d^2v_x}{dz^2}$ both go to zero because we assume that the equation is invariant under translation. This leaves us with a single equation.

$$\frac{dp_x}{dx} = \mu\left(\frac{d^2v_x}{dx^2}\right) \quad (6)$$

Integrating equation (6) two times with respect to z we get equation (7) which is known as Poiseuille flow.

$$v_x(z) = \left(\frac{1}{\mu}\right)\left(\frac{dp_x}{dx}\right)\left(\frac{z^2}{2}\right) + Cz + D \quad (7)$$

We now examine the boundary conditions required by the no slip condition. No slip means the flow velocity at each of the plates is zero or, $v_x(z=0)=0$ and $v_x(z=b)=0$. The first condition determines the value of D to be 0. Then, the second condition says that $C = -\left(\frac{1}{\mu}\right)\left(\frac{dp_x}{dx}\right)\left(\frac{b}{2}\right)$.

Substituting these two conditions into equation (7) gives us $v_x(z)$.

$$v_x(z) = \left(\frac{1}{2\mu}\right)\left(\frac{dp_x}{dx}\right)\left(z^2 - bz\right) \quad (8)$$

Next we calculate the average velocity in the x direction $\langle v_x(z)\rangle$ which is done by integrating equation (8) from 0 to b and dividing by b. After some algebra the result is the following.

$$\langle v_x(z)\rangle = -(\nabla p)\frac{b^2}{12\mu} \quad (9)$$

Equation (9) is known as Darcy's Law and governs the flow of the fluid in a Hele-Shaw cell; it is also an assumption made to derive the results found in Lee's paper.

2.3 Self-similarity and Scaling during Bubble Break-off

A number of papers that explore different break-off events have been published with varying results. In general these papers characterize break-off with a scaling law relating the neck thickness to the time until break-off occurs. If such a law is found then a process is said to be self-similar. Self-similarity means that there is a part of the interface that can be rescaled to a time-invariant shape. Generalized scaling laws take the form $f(x) \propto t^{\alpha}$. In the case of linear scaling, $\alpha = 1$, the outer bubble interfaces approach each other with a constant velocity as the neck thins towards break-off.

Burton found a scaling with t for bubbles of nitrogen breaking off from a nozzle in a viscous fluid of high viscosity and a scaling with $t^{1/2}$ for surrounding liquids of low viscosity [4]. In the case of aligned ^{3}He crystals merging near 0.32 K Ishiguro found a scaling law of $t^{1/3}$ [5]. Bergmann found that break-off events involving an air bubble breaking off in water is not strictly self-similar, but in a limiting case they found a $t^{1/2}$ scaling [6]. Cohen confirmed self-similarity for the case of a two fluid drop snap-off problem in which both fluid viscosities are large and approximately the same [7]. Zhang extended these results to account for viscosity ratios ranging from 1/16 to 16 [8].

Unlike this paper, most published results, such as all those listed in the previous paragraph, explore bubble break-off in a three dimensional regime. A couple papers exploring phenomena in a Hele-Shaw cell observed break-off events, but it was not the topic of their studies [9], [10]. To my knowledge there are no systematic studies of bubble break-off in a quasi two-dimensional setting.

2.4 Lee *et al.*

Lee's paper predicts bubble break-off in a Hele-Shaw cell is a self-similar process [1]. Lee has provided a functional representation of the break-off region with constants to account for scale, symmetry and drift. The purpose of our experiments is to discover and explore the extent of the physical parameters in which this theory is correct.

Lee's model makes strictly non-physical assumptions including surface tension equal to

zero, incompressibility of both fluids, and zero viscosity for one of the two liquids (the air). All three of these assumptions are not true in the physical world; however, approximations can be achieved by choice of fluids and experimental parameters.

Lee places constraints on the conditions of the bubbles before and after break-off. The theory requires that the bubbles maintain equal pressure before and after break-off occurs. This condition means that instead of having two separate bubbles after a break-off, it must still be one connected domain of air after separation so it is clear the bubbles are still at constant pressure. This has been the most difficult condition to meet for reasons that will be explained in section 3.2.1.

Lee *et al.* suggest an experiment in their paper to satisfy these conditions. They begin with a single air bubble in a Hele-Shaw cell that contains two inlets through which air may be withdrawn as shown in Fig. 4. They connect these two inlets to the same pipe and withdraw air through both inlets until the two bubbles are sufficiently small that they are required to separate. In theory this would be a convenient way to observe this phenomenon; however, in the course of our experiments we found this approach to be impractical (see Methods 3.1 for a further explanation). Therefore, in order to meet this restraint we created an annulus of air in oil and then caused a single break-off event to occur so that a simply connected air bubble remained and thus the equal pressure condition was satisfied.

In this theory, under an assumption that the region of break-off is much smaller than the size of the entire bubble, a linear scaling law is predicted for before break-off. That is the interfaces should approach with a constant velocity. In a personal communication with Eldad Bettelheim, the second author of Lee's paper, we were told that if this assumption is not met then the break-off is still self similar but they didn't know how to write the solution explicitly.

2.5 Viscous Fingering and Bubble Break-Off

Both ease of experimentation as well as relevance to the petroleum industry have fueled extensive research on Hele-Shaw flows. A sizable portion of this research explores viscous fingering, which results from pumping less viscous fluid into a more viscous fluid [11]. The term "viscous fingering" describes the finger-like instabilities that penetrate the more viscous fluid resulting from this injection. This phenomenon causes a problem for oil companies because as oil is withdrawn from a reservoir water replaces it and viscous fingering occurs since

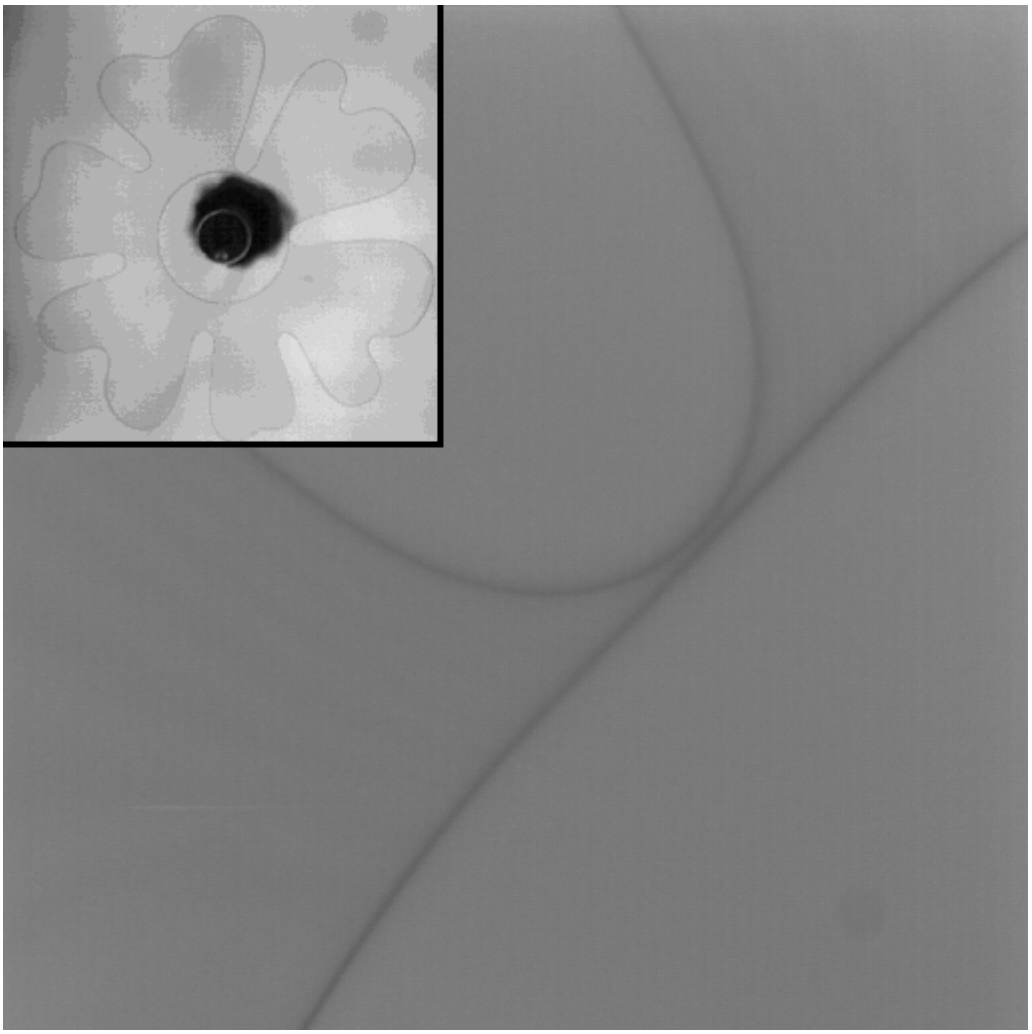

Figure 3: (Top of next page) The inset in this figure shows the shape of the whole bubble as viewed from above just before break-off. Note that the gray in the inset indicates oil, white is air and the inlet is the black circle in the middle. The break-off occurs when the expanding circle of oil comes in contact with the outer edge of the annulus. The shape of the entire bubble, rather its connection before and after break-off is important so that the theoretical constraint of equal pressure bubbles is met before and after break-off occurs. The larger picture is a close up of the region within the dotted-line box in the inset and shows experimental data of a bubble just before break-off.

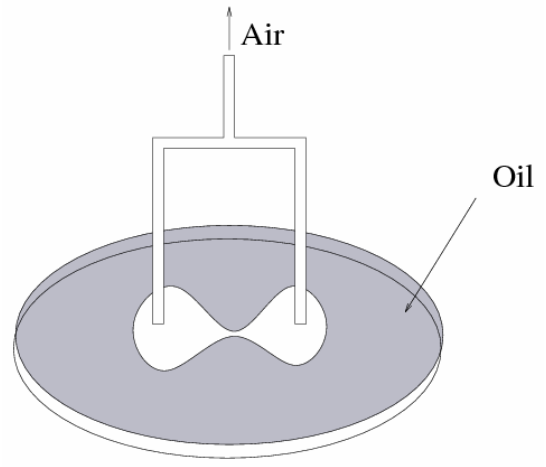

Figure 4: This figure is taken from Lee's paper and diagrams their proposed experiment [1]. Air (white) is being withdrawn through a pipe from a two-dimensional air bubble that is surrounded by oil (gray). As the amount of air is reduced, the bubble is forced to break-off into two separate bubbles, but they still remain connected and at equal pressure due to their connection through the extraction pipe.

water is less viscous than oil. Fingers of water are pulled towards the point of extraction and when they reach the outlet further pumping will yield more and more water since it is much easier to pump (less viscous). This phenomenon lowers the efficiency of pumping operations with respect to how much oil can be economically removed from a reservoir. Oil companies are interested in any information that could lead to innovations that limit or prevent viscous fingering all together. Experiment and theory have been able to describe aspects of viscous fingering through selection rules such as finger width [12] and fjord angle [13], but our understanding of the phenomena is far from a complete theory.

Bubble break-off is not the result of an interfacial instability as is the case with viscous fingering. The process of break-off involves oil being pumped into an area of air so the interface remains stable. Viscous fingering still plays an important role in this paper because there are unstable interfaces present—but not directly involved in the process of break-off. While viscous fingering and bubble break-off differ intrinsically in their underlying physical mechanisms, they both belong to a more general phenomenological category called Laplacian growth (LG). This link with viscous fingering provides a practical reason to study bubble break-off. An understanding of bubble break-off contributes to the understanding of LG which in turn may enhance our understanding of viscous fingering and thus draw the attention of a multi-trillion dollar industry. Some experiments have even found that bubble break-off occurs as a part of

viscous fingering [10]. In addition to these contributions, viscous fingering also provided the most effective method I found for setting up a range of initial conditions that result in a break-off event, as explained in the section 3 (Methods).

Methods

3.1 Experimental Apparatus

3.1.1 Experimental Approximations to Theory

In the formulation of his theory Lee makes non-physical assumptions. He assumes that the air and oil are incompressible, the air has zero viscosity, the system is strictly two dimensional and that surface tension is zero. In general oil is assumed to be incompressible except for situations of extreme pressure, and air is generally assumed to be compressible except for when very small pressures are used as in out experiment. The dynamic viscosity of air, $\mu_{air} = 1.8 \cdot 10^{-5}\, kg/m \cdot s$, is also much smaller than oil, $\mu_{oil} = 1 \cdot 10^{-3}\, kg/m \cdot s$, so it can be approximated to be zero. The assumptions that are of primary concern are that the theory is strictly two dimensional and assumes surface tension is zero.

In the zero surface tension limit the capillary number is infinite. Capillary number, Ca, is defined to be the dynamic viscosity times velocity divided by surface tension: $Ca = \mu v / \sigma$ [3]. This non-dimensional parameter is often the primary factor of interest for Hele-Shaw flows, and in any physical system it is finite. It is impossible to achieve this limit experimentally; however, we are able to increase the capillary number by increasing pump rates (velocity) and the oil viscosity. By changing these parameters the effects of surface tension are minimized.

Hele-Shaw cells present a quasi-two dimensional systems, but it is not the strictly two dimensional case ideally presented in Lee's paper. In a Hele-Shaw cell experimentalists approximate a two dimensional system by making the length scales of interest much larger in two dimensions than the third. In the case of bubble break-off this means that we can't apply the theory to a region close to the point of break-off because it is always a three dimensional interaction in this region (see Fig. 18 for a comparison of interface separation and the gap thickness b). By making the gap thickness, b, smaller this region can be reduced in size.

3.1.2 Apparatus Design

For a detailed description of the radial cell used I direct you to Mitchell Moore's PhD thesis since he is the one who designed and constructed it with Eran Sharon [14].

We designed and constructed a rectangular Hele-Shaw cell with the intent of performing the experiment described by Lee and shown in Fig. 4 [1]. Because this project was on a timeline

we strived for a balance between convenience and practicality. In this spirit most materials were either scrap on hand or cannibalized from older experiments. Only the spacers and 7-inch clamping bolts were bought specifically for this experiment.

After reviewing the literature to get a feel for the primary components of a Hele-Shaw cell, we chose guidelines for our cell. We chose to make the plates out of Plexiglas because it is cheaper and easier to work with than glass and we had a large 3/4" thick sheet available—thick enough to avoid flexing at the intended pumping rates. For image lighting we chose to use backlighting with LEDs instead of the top lighting apparatus specified in Moore's dissertation [14]. With backlighting it is much easier to obtain a uniform light distribution. The frame and clamps for the cell were taken from the linear cell described again in Moore's thesis and modified appropriately.

The design of the interior of the cell was chosen to minimize the number of parts needing to be machined. With this in mind we chose to make both cell inlets and the cell buffer all in one plate of Plexiglas, as shown in Fig. 5, leaving the other plate of Plexiglas completely untouched. In general cutting this much material out of the sheet would bring up concerns about pumping rates flexing the cell, however we did not intend the cell to be used at high pumping rates for this experiment.

Below are schematic drawings of all the pieces needed to assemble the rectangular Hele-Shaw cell. In these drawings each grid is 1/2 an inch on a side and all features that occur off of grid lines or intersections are at half square increments (1/4 inch increments). Figure 5 shows the bottom plate of the cell; the top plate is just a 12 in. by 12 in. by 3/4 in. sheet of Plexiglas. The bottom of Fig. 5 is a drawing of the inlet profile, and Fig. 6 and 7 show all parts of the frame used for clamping the cell.

The cell design worked pretty well, but if I were to make another I would put half the buffer in each plate and move the inlets closer together for reasons discussed in section 3.2.2. After I had milled out the buffer section and I was milling the o-ring groove I had difficulty obtaining a uniform depth. I assume this is due to the relaxation of the Plexiglas plate from milling out the buffer; splitting the buffer between the two plates could reduce it.

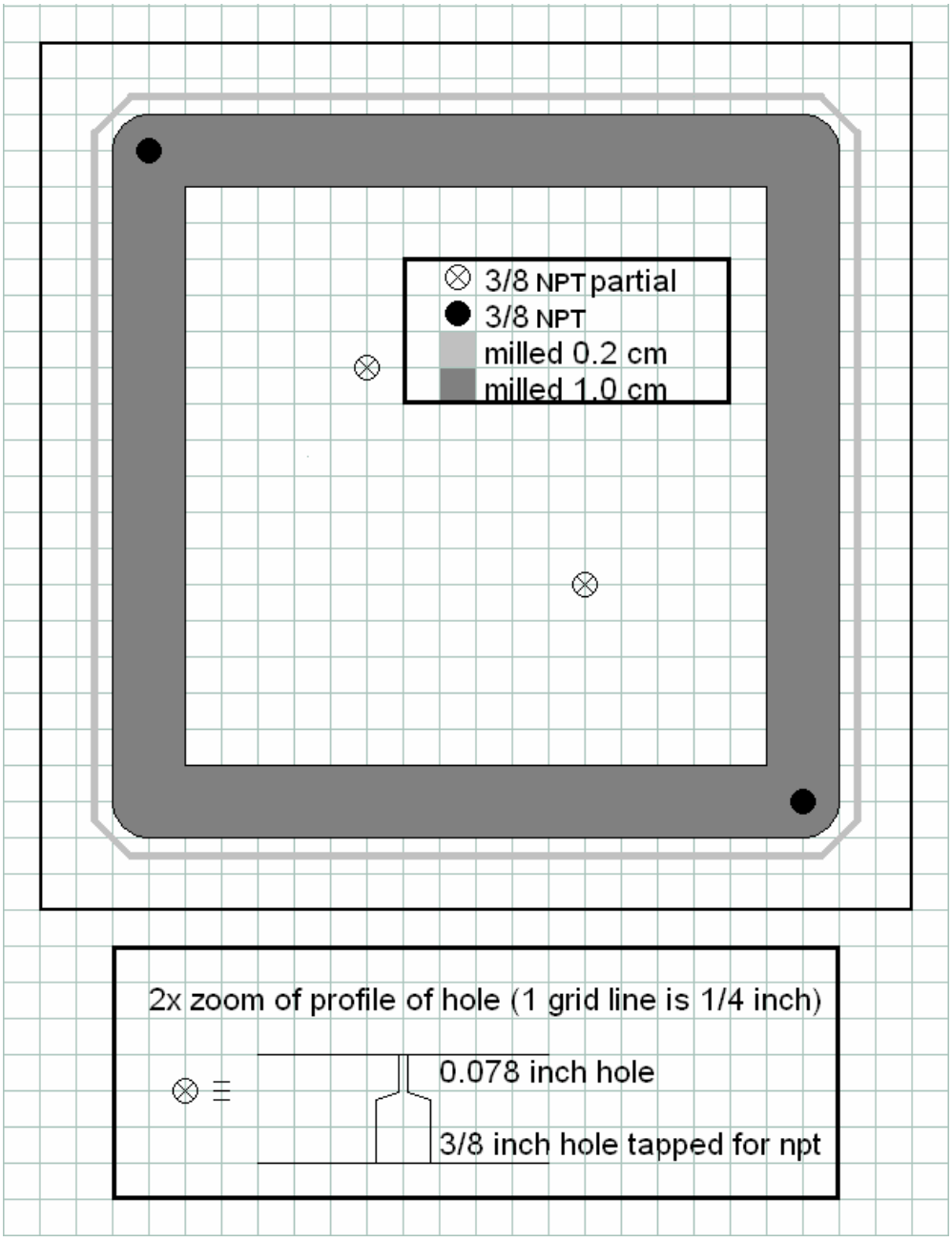

Figure 5 (top): This is a diagram of the bottom 3/4" thick Plexiglas plate of the rectangular Hele-Shaw cell drawn to scale. Each grid box is 1/2 inches on a side. The ⊗ symbol denotes a hole, which is tapped for 3/8-inch NPT for 1/2 inch from the bottom side of the plate toward the top, and the remainder of the hole is 0.078 inches (see bottom of this figure). The ● symbol denotes tapped 3/8-inch NPT holes through the sheet of Plexiglas. The light gray is the small groove used to set the O-ring; this groove is 0.2 cm deep and 0.16 inches wide centered along a line 0.75 inches from the edge of the cell. The dark gray is the deep groove used as the Hele-Shaw cell oil buffer it is 1 inch wide and 1 cm deep; the outside corners are rounded with a 1/2 inch diameter from the 1-inch milling bit used. **(bottom):** This is a profile of the holes drilled into the 3/4" Plexiglas sheed marked with ⊗. The top plane of this figure corresponds to the top of the plate as shown in Fig. 5 (top) so these holes were drilled from the bottom of the plate.

In addition to the components shown in these figures there are three additional components used for lighting. A 10 by 10 inch square of 0.15 inch thick diffusive plastic with four 3/8ths inch holes cut out to fit the cell inlets was made. This plate is held in contact with the bottom Plexiglas plate by the NPT connectors for the two gap and buffer inlets. Then for lighting I placed a 32 by 33 array (approximately 9.5 by 9.5 inches) of LEDs below the diffusive panel resting on the table. The third component was a 5-amp 20-volt power supply. This provided semi-uniform lighting in the region of interest; however, the led panel had a circular hole in the middle since it was made for another experiment and this created a dim area in the center of the cell. While this kept the images from being uniform it was still bright enough in this region and background subtraction was able to remove this discrepancy.

3.1.3 Silicone Oil

All experiments presented in this paper use the same two fluids—silicone oil and air. The silicone oil was purchased from Clearco Products Co., has dynamic viscosity $\mu = 1 \cdot 10^{-3}\, kg/m \cdot s$, and nominal surface tension $\sigma = 20.9 dynes/cm @ 25^{o} C$. As a point of reference, this silicone oil has a dynamic viscosity about 100 times greater than water.

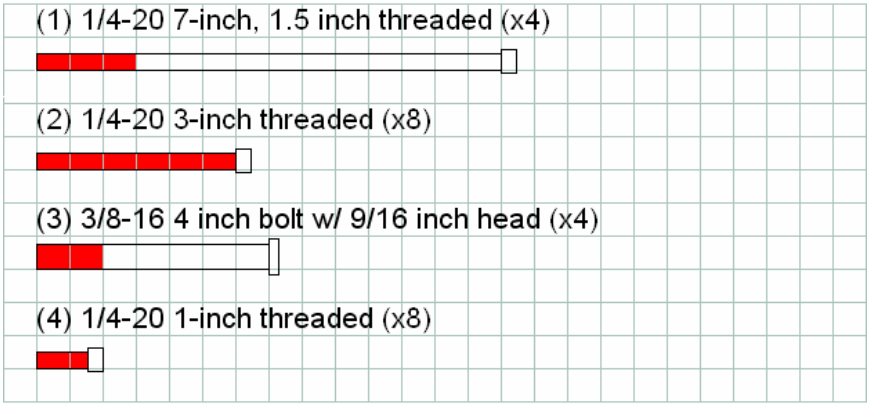

Figure 6: This figure shows all of the bolts and quantities used to assemble the cell. Again the grid scale is 1/2 inch/grid and the red areas are the bolt lengths that are threaded. The number labels are used in later figures to show where each bolt is.

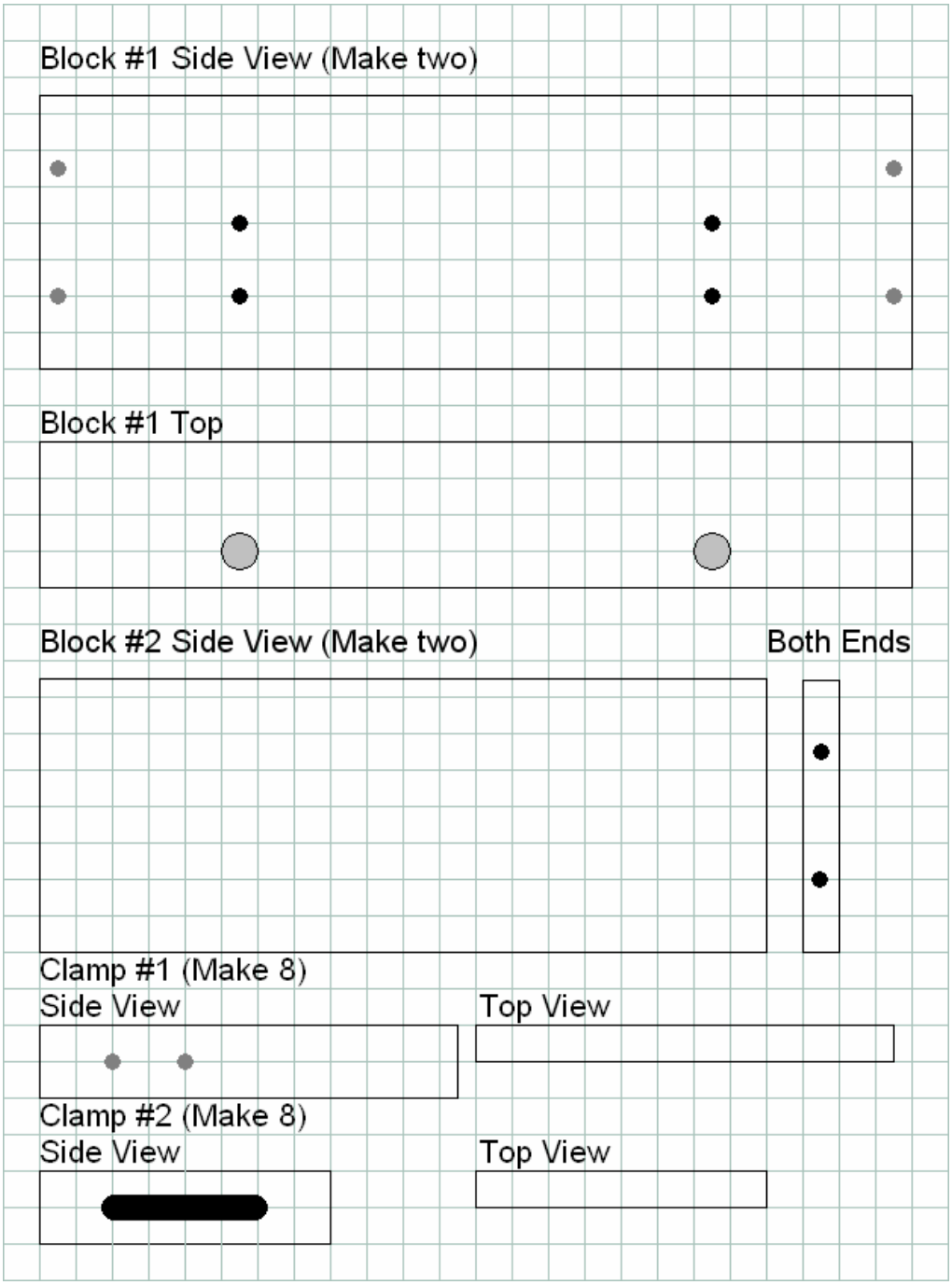

Figure 7: This figure shows all pieces used to assemble the Hele-Shaw frame. Again all pieces are drawn to scale with each grid box being 1/2 inch on a side. All lines and holes that fall inbetween gridlines are intended to be at 1/2 square increments (or 1/4 inches from the nearest grid line)—no smaller fractions are used. The ● symbol on the first block and first clamp denote 1/4 inch holes all the way through the material drilled so that 1/4-20 inch optical bolts can be flush mounted. The ● symbol on blocks #1 and #2 denote 1/4-20 tapped holes 1-1.5 inches deep. The ◯ symbol denotes 3/8-16 tapped holes 2 inches deep. The black area on the "Clamp #2" is a 3/8ths inch hole all the way through the clamp that runs 2 inches (center start to center end is 2 inches so the rounded parts extend beyond 2 inches).

3.1.4 Apparatus Assembly

Figure 8, below, shows the completed Hele-Shaw cell, and I will provide step-by-step instructions as well. Throughout the instructions refer to this figure. Pieces of the cell as well of the bolts will be referenced according to their labels in Fig. 6 and 7. The cell also sits on an optical table which has 1/4-20 inch holes every 1".

1. Both of Block #1's and #2's are joined into a rectangle via the outer most holes in Block #1 and the threaded holes in the end of Block #2 using eight (2) bolts.
2. Four Clamp #1's are attached to the side of Block #1 with two (4) bolts each (8 bolts total).
3. At this point the LED array should be lowered into the interior of the rectangle. Note that a 1" diameter hole should be placed on the side of one of the #2 Blocks so that the LED array power wires as well as the pipes can be passed to the outside of the cell.
4. With the pipes attached to the bottom Plexiglas plate as shown in Fig. 9 place the plate groove side up making sure to feed the pipes out the hole cut in Block #2.
5. Arrange the spacers (12 inch x ½ inch x 0.015 inches) on top of the bottom plate as shown in Fig. 8 in light gray along the perimeter of the cell. Note that each spacer has one end that will extend 1/2 inch beyond the edge of the cell. We could have cut these down to 11 1/2 inches each to avoid this, but that can cause a barbed edge on the spacer that might change the gap or cut into the Plexiglas.
6. Install a 0.11-inch diameter O-ring into the small groove of the cell.
7. Place the second Plexiglas plate on top of the first being careful not to move the spacers or O-ring.
8. Install the remaining clamp components: 4x Clamp #1, 8x Clamp #2, 4x (3) bolts, and 4x (1) bolts as shown in Fig. 10.

This concludes the cell assembly and the experimental procedures for break-off will be detailed in the following section.

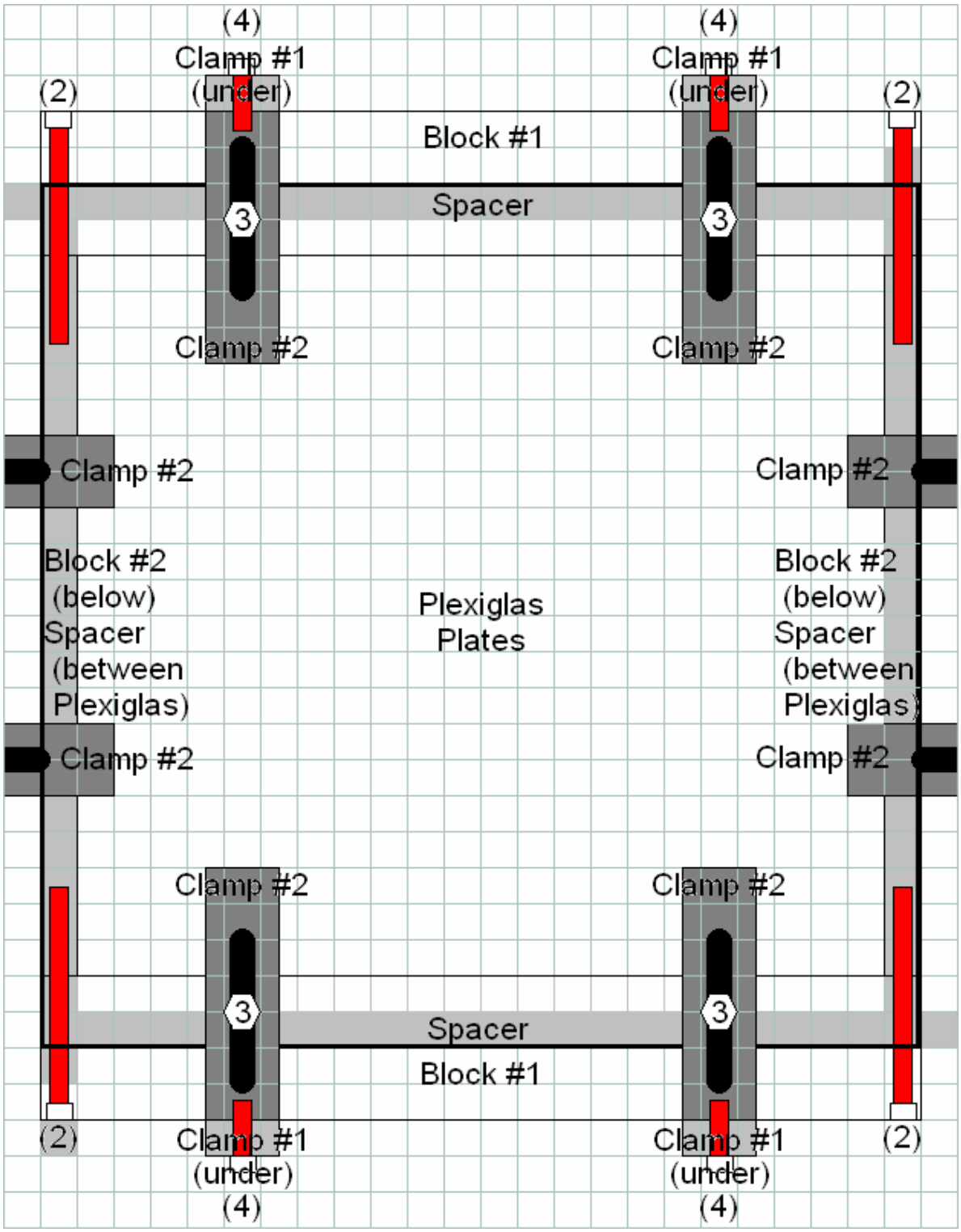

Figure 8: This is a diagram of the assembled cell. For construction details please refer to the text.

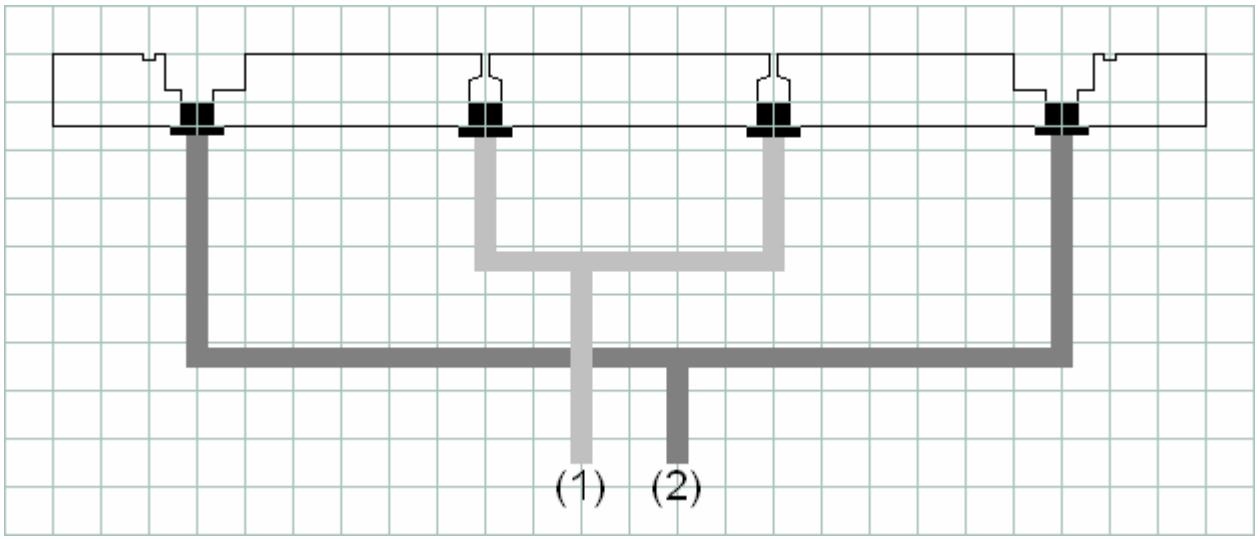

Figure 9: This is a schematic drawing of the Hele-Shaw cell cross section along the diagonal containing all four inlets. In actuality the lengths of piping from each inlet to the joint are equal, but the image was drawn this way so that the connections were clear. Note that the horizontal scale of this image is really $1/\sqrt{2}$ inches/grid since the cell is $12\sqrt{2}$ inches along the diagonal.

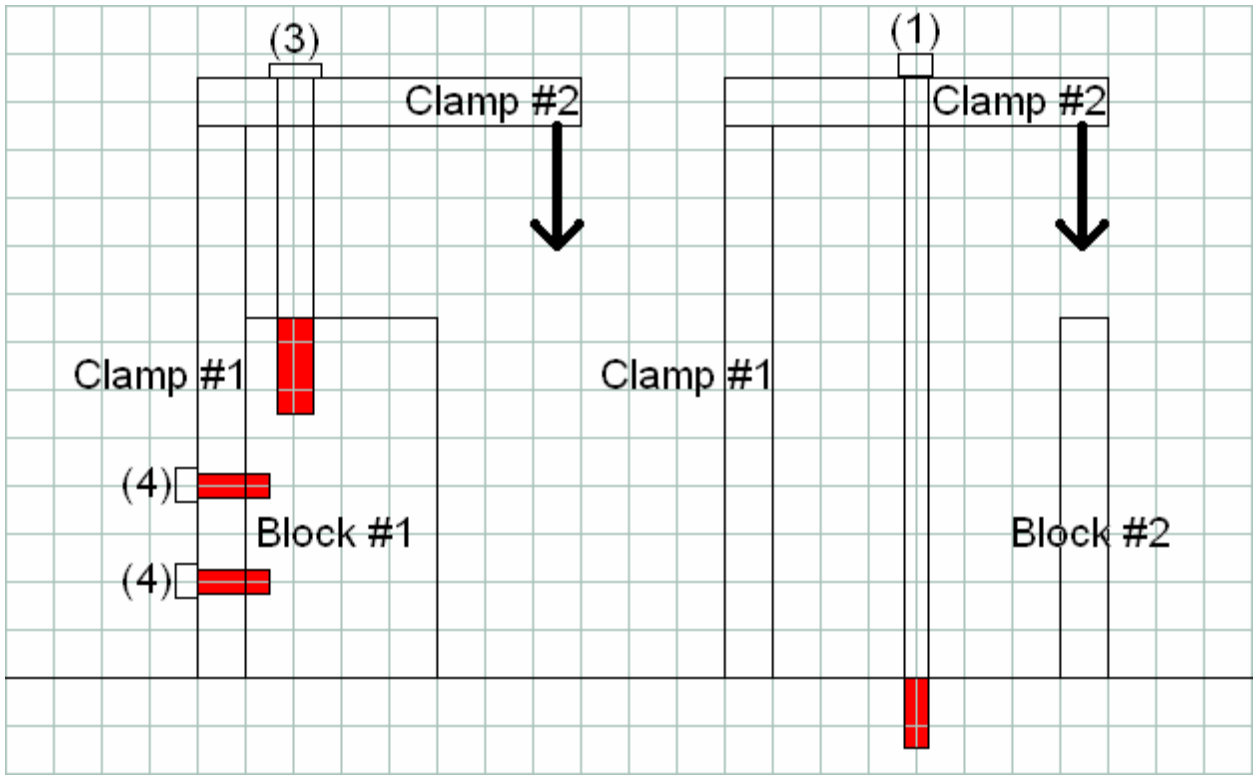

Figure 10: **(Left)** a schematic drawing of the four clamps shown at the top and bottom of Fig. 9. **(Right)** A schematic drawing of the four clamps shown going off the left and right edges of Fig. 9.

3.2 Procedure

3.2.1 Rectangular Cell and Lee's Experiment

While no break-off events that met Lee's conditions were observed in the rectangular cell using his suggested experiment, a description of the attempted procedures is included.

I attempted two distinct methods to obtain bubble break-off as described in Lee's experiment shown in Fig. 4 [14]. I will explain these two methods as well as the problems I had with each. For this discussion the cell inlets will be labeled and referred to as shown in Fig. 11. In all experiments including those in the radial cell the cell is completely filled with 100 cS silicone oil before any experiments are conducted; it is also important to remove any air bubbles from the gap and buffer in order to accurately measure pumping rates. Also, because testing in this cell was preliminary most pumping was done by hand. I attempted the same processes with the automated syringe pump and obtained the same results.

The size of the cell and distance between the two interior inlets, (2) and (3), posed the largest problem for this experiment—particularly for setting up the initial conditions. The initial conditions presented in Lee's paper involve a single bubble of air inside the gap that encloses two inlets through which air can be removed. I saw two options to achieve this goal and both encountered the same problem. I can grow a single circular bubble from one inlet until it encompasses both inlets or I grow two circles, one from each inlet (2 and 3), until they merge. If

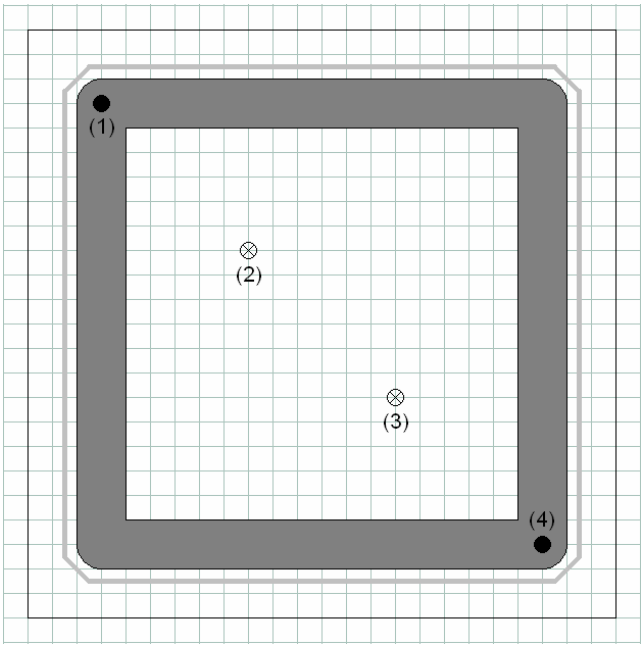

Figure 11: Inlet number labels used for procedural discussion.

I closed off inlet (2) and slowly pumped air into (3) then a circle of air would form centered on (3) and unfortunately due to the cell design the bubble comes in contact with the buffer before it passes the second inlet. If I grow two bubbles slowly they still leak to the buffer before they connect.

Eventually I was able to connect the two bubbles by means of viscous fingering, but this was not a reliable process. If I grew two circles centered at inlets 2 and 3 until they were nearly touching, not yet in the buffer, and then pumped air into the gap quickly sometimes a finger would form between the bubbles and connect them without letting the bubble into the buffer. However, as stated before, this process was very unreliable and in more cases than not resulted in one or both of the buffers leaking to the buffer.

In the rare cases in which I was able to obtain the required initial conditions, there were further problems. When I removed air through both inlets (2 and 3) the bubbles would in fact break-off, but not in the region between the inlets, but rather *at* one of the inlets. While I have the control to make the bubble break-off, I had no power to choose *where* the break-off occurs. At best I could observe one side of a break-off as it broke off into one of the inlets. While this procedure meets the condition that the bubbles maintain equal pressure throughout the process, half the bubble is not longer visible after break-off occurs. In other cases bubble break-off would occur between the two inlets, but in these cases there were multiple break-off events and I was unable to tell which occurred first, meaning that in those cases I wasn't sure if the equal pressure condition was met.

In light of the difficulties controlling where break-off would occur, I chose to take a different approach to the experiment. Instead of withdrawing air from two places within one bubble I concocted a procedure that limited break-off to a narrow annular region surrounding the inlet and in many cases to an even smaller area. While this experiment could have been conducted in the rectangular cell that I built, we decided to move to the radial cell constructed by Moore because it has a more uniform gap [14].

3.2.2 Radial Cell Procedures

This section describes the procedure that was used to obtain the data reported in this thesis. The goal was to create an annular domain of air in oil and then cause a break-off event of the annulus. This guarantees that the bubbles maintain equal pressure before and after break-off. However

this poses the question about the withdrawal of air being a result or an assumption of Lee's theory. The answer to this question will be discussed in the Results section 4.1.

The radial Hele-Shaw cell used has three inlets that we used. One in the top of the buffer used to remove rogue air bubbles. The second in the middle of the buffer for pumping oil in or out and a third in the middle of the bottom plate, which can be connected to a jar of oil or atmosphere through a 6-inch tube. Pumping oil into or out of the buffer does all pumping. For simplicity I sometimes refer to pumping into the gap inlet; this means that I am withdrawing oil from the buffer and vice-versa for withdrawing oil from the center inlet. Here is the general procedure for obtaining a break-off event.

1. Begin again with the Hele-Shaw cell filled completely with 100 cS silicon oil and the gap inlet tube open to atmosphere.
2. Withdraw about 20 to 40 mL of oil from the buffer. This sucks an equivalent amount of air into the gap and buffer. The volume of the gap is small so 20 mL should be more than enough to get air into the buffer. Getting air into the buffer is not the point; you just need to fill the gap with a significant amount of air. If you can stop the pump at the correct time and fill the gap and not get air bubbles in the buffer, then skip step 3.
3. Follow the procedure outlined in Moore's thesis for removing air bubbles from the buffer [14]. That is, tilt the cell, open the top buffer valve, remove oil from the buffer until all the buffer bubbles are connected, pump oil into the buffer until the large bubble is completely expelled, close the top valve and lower the cell.
4. Once the buffer is bubble free and the gap has a significant amount of air in it put the gap inlet tube into a jar of oil and pump oil into the buffer at the maximum speed (105mL/min) until air bubbles stop coming out of the tube. For unknown reasons this procedure results in a small air bubble being trapped in the top of the tube near the gap inlet—exactly the conditions needed. I suspect that this happens because air gets caught in some of the pipe connections out of the main fluid flow but regardless it was a fortunate side effect of adding the pipe to the cell.
5. The cell is now ready to rapidly repeat the experiment. By setting the automated pump to a constant rate between 0.01 and 5 mL/min an annulus of air will grow and then break-off. For more control over the break-off conditions this procedure can be broken into three steps.

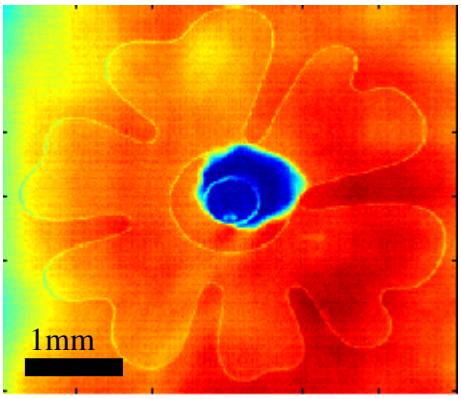

Figure 12: This is a sample viscous fingering pattern formed to set the initial conditions of a break-off event.

a. After the size of the trapped air bubble is known, pump about half of the air bubble into the cell at a slow rate, approximately 0.1 mL/min, so that you obtain a nearly circular bubble. As will be shown, increasing or decreasing the amount of air pumped in at the slower rate will decrease or increase the curvature of the inner and outer interfaces at break-off.
b. Increase the pump rate to a value greater than 0.2 mL/min and, as many papers have shown, viscous fingering will occur at the annulus's unstable outside boundary between the oil and air. This will cause a pattern similar to that in Fig. 12.
c. After the entire air bubble has been pumped change the pump rate again to the rate at which you want break-off to occur. Then a circle of oil will grow and come into contact with one of the stationary fjords of the radial fingering pattern. This circle of oil is stable because a more viscous fluid is being pumped into a less viscous one.

To repeat the experiment just pump the air bubble back into the tube and repeat steps 5(a)-(c). Conveniently enough, break-off occurs in roughly the same position in the cell every time due to the fingering pattern taking its shape due to the mechanical noise inherent to our inlet. Lajeunesse and Couder also observed this phenomenon in their paper on tip splitting of viscous fingering [15].

Though a partial explanation of how to manipulate the initial conditions was given above I will provide a clearer account here. Basically 5(a) and 5(b) determine the inner and outer curvatures of the interface at break-off and 5(c) determines the pump rate during and after break-

off. In a comprehensive study of bubble break-off (this is not one) these are important parameters to vary to examine a full range of events.

Interface curvature can be varied in three ways. The curvature of the inner interface is completely determined by the distance from the inlet because its interface is stable during pumping so it is always a circle. This distance is directly proportional to the amount of air pumped in at the small (small defined to be small enough for the outer interface to remain stable/circular) in step 5(a). Skipping step 5(a) completely and creating fjords close to the inlet can obtain a maximum inner curvature and skipping step 5(b) and creating two nearly concentric circles may obtain a minimum inner curvature. Then almost entirely independent from the interface curvature set by steps 5(a) and 5(b), step 5(c) determines the pump rate at the time of break-off.

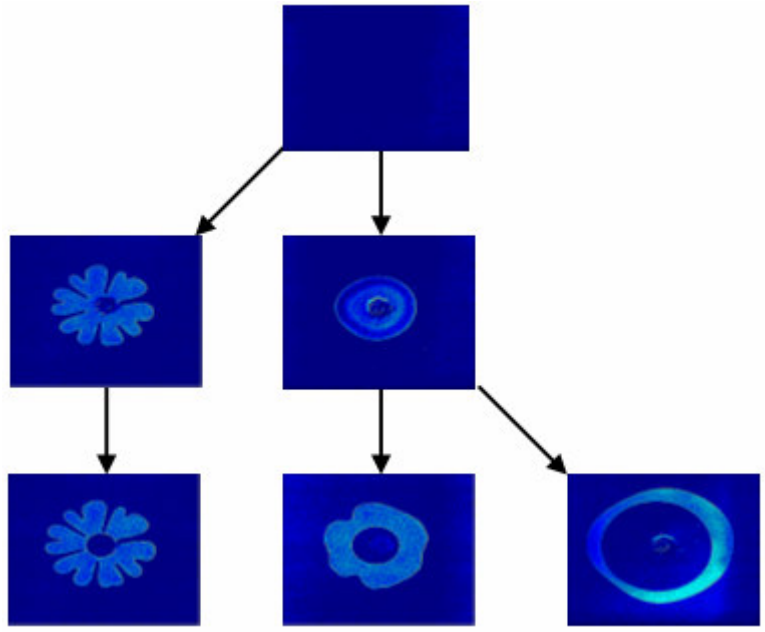

Figure 13: This figure shows images of the initial conditions I achieved with the methods described above. Starting at the top in which the entire cell is filled with oil the left arrow is for high pump rates (>about 0.2 mL/min) and the down arrow is for low pump rates (<about 0.1 mL/min). The bottom right image continues the same pump rate started in the upper left image. Again at the split from the center image to the center bottom image is for high pump rates and the bottom right is for low. In the end this process produces two highly curved interfaces at break-off (bottom left), two moderately curved interfaces (bottom center) and two nearly identical curvatures (bottom right)

In a comprehensive study of bubble break-off interface curvature and pump rate are two very important parameters to vary and this procedure provides the means to do so. The theory provides solutions for this range of curvatures and pump rate is important in deciding if surface tension is contributing to the break-off. For an example of the range of initial conditions available see Fig. 13 above.

3.2.3 Imaging

All experimental images were taken using a Vision Research Phantom v4.0 camera mounted vertically above the cell. We used an Olympus OM-System Zuiko MC Autos-S lens with a focal length of 50 mm and f = 1.8. We also used a set of Olympus bellows (extension tubing) to increase the lens magnification. Overall we obtained a viewable square that is 2.8 mm on a side. This camera is capable of taking between 20 and 1000 frames/second at full 512 x 512 pixel resolution and saves a large cache of pictures (several thousand).

Using the Image Research camera software I set the camera to save images from 1 to 2 seconds on either side of when I trigger the save. With the camera and lighting set up appropriately I begin the experiment and trigger this camera to save as soon as I observe break-off so that the saved file would contain sequences of images both before and after break-off. This method allowed me to select an appropriate time range of data collection, but may need some tweaking to account for individual reaction speeds.

3.3 Data Analysis

3.3.1 Image Analysis

In this section I will demonstrate the complete image analysis process used to extract the oil-air interface from experiment and compare it to theory for a single image. Analyzing a set of images consists of creating loops and using a couple different functions with parameters from the first image to assure that all images are edited in the same manner. In this section I focus on the results of the MATLAB code and not specific function calls; for a summary of all the functions used to analyze this data see Appendix A.

Beginning with an image obtained from the Phantom v4.0 camera I threshold the entire picture based on the average intensity value. I begin by setting this threshold equal to the mean value and increase it until no remaining pixels fall outside of the interface as shown in Fig. 14.

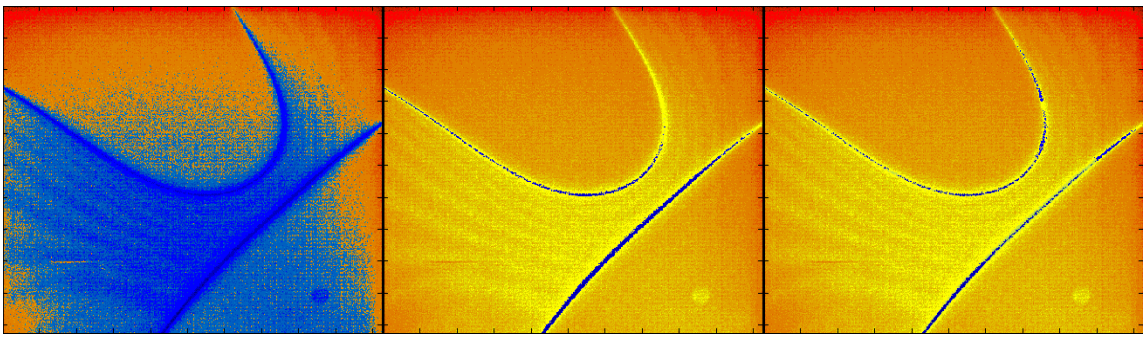

Figure 14: (Left) The blue points are all points extracted by a mean intensity value threshold. This means that all points in blue are below the average intensity value in the image. (Middle) This is the same image but the threshold has been lowered to 16 intensity values below the mean value so that all points lie on the line. **(Right)** In this image the intensity threshold process shown in the left and middle panels has been repeated for smaller and smaller rectangles in areas where the initial threshold missed the interface. In total 12 local value thresholds were used.

In order to extract the interface further analysis must be performed. The process described above yields two arrays: the x and y coordinates of the points that lay on the interface. The theoretical interface functions define the break-off neck to be along the x-axis and it also defines parameters based on the curvature of two interfaces. In order to do this the interface must be separated into two interfaces and rotated to the correct orientation. The interface must also be cropped to a region near break-off because it is clear that the theory, which predicts parabolic interfaces prior to break-off doesn't apply to about 2/3rds of this picture.

Because time was an issue in this project these jobs were performed more or less manually. I find the rotation angle by looking at a plot of the two images and rotating it until the bottom interface looks level. This process is done manually for the first image, but then the same angle is used for all subsequent images. After rotation is complete the interface is manually centered and cropped. First the user is asked to click on the image "center" meaning the point of break-off. Once this point is selected the user is asked to crop the image to a rectangular region specified by the lower left *(x, y1)* point and the upper *y*-coordinate, *y2*. This function uses *(x, y1)* and *(-x, y2)* as the lower left and upper right points to define a rectangle and removes all other points from the interface because the image is centered and we want a symmetric window. Finally a more precise centering is done by computing second order polynomial fits of the two interfaces and averaging their vertices. A rotated, cropped and centered interface is shown in Fig. 15.

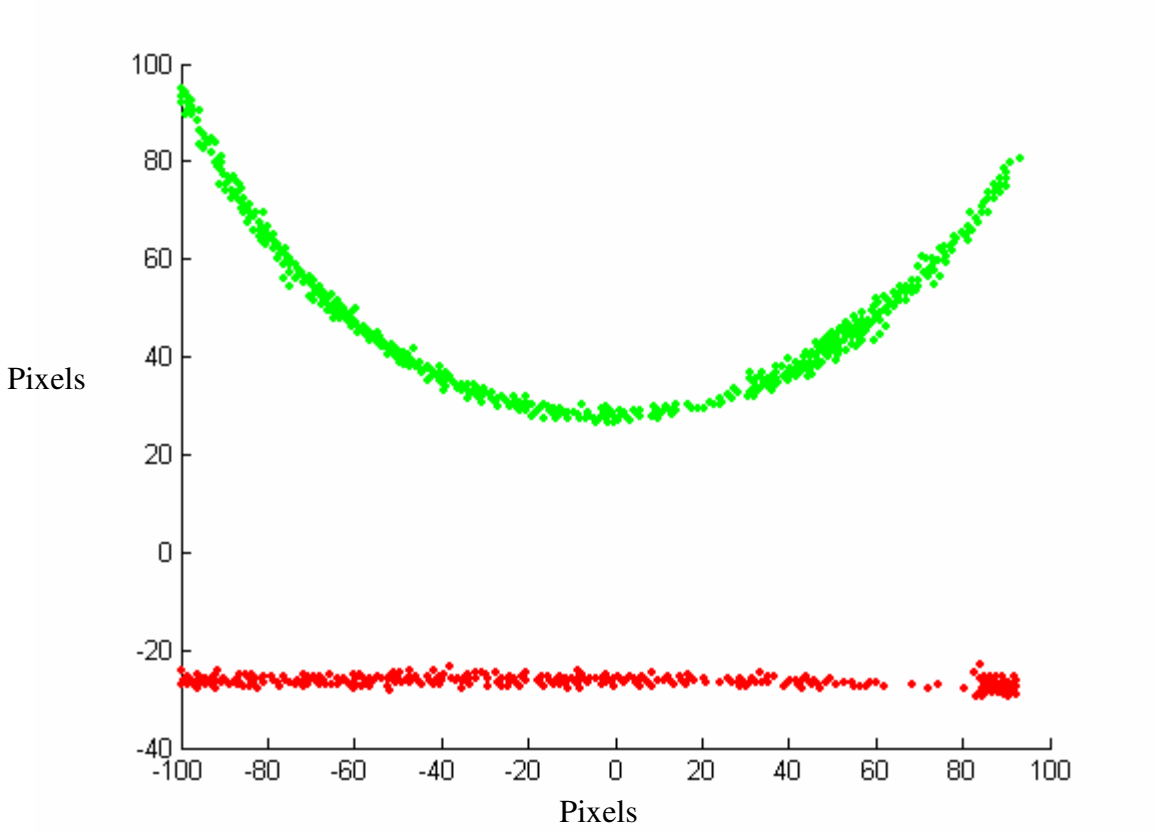

Figure 15: This is the interface after rotation, cropping, and centering. At this point it is ready for a proper rescaling and comparison to theory. There are 60 pixels for each millimeter in this image.

3.3.2 Comparison to Theory: A Correct Fitting of Theoretical Parameters

With the extracted interfaces in hand I now turn to the theory provided by Lee *et al.* This theory provides two equations—one for before break-off and one for after break-off. In their given form they are not in laboratory variables, but I have converted them into lab variable, with the exception of time, which is still in units of length.

$$y = x^2(c \pm a) \pm t + \gamma t \qquad (10)$$

$$y = x^2\left(c \pm a\sqrt{1+\frac{2t}{ax^2}}\right) + \gamma t \qquad (11)$$

Three parameters, a, c, and γ, and a rescaling of time are needed to fit the theory to experimental data. For an arbitrary choice of parameters, a time evolution of the interface is in Fig. 16.

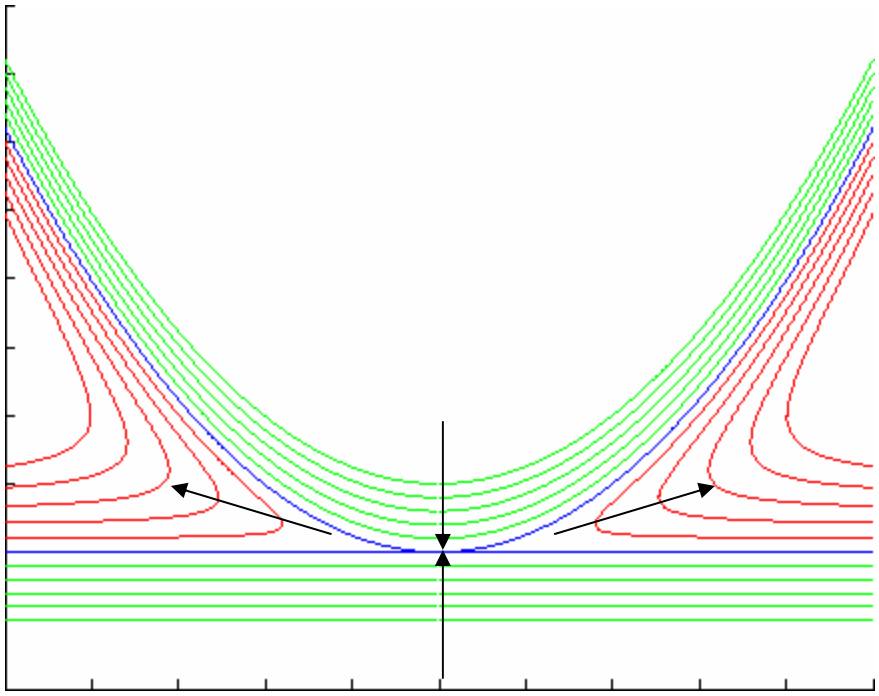

Figure 16: In this arbitrary fitting of parameters, c is approximately the same as a and γ is zero. This means that the two parabolic curvatures before break-off are $2a$ and 0 so one is a parabola and one is a flat line. In the image the green lines show the interface before break-off, the blue line indicates the instant of break-off and the red lines are the interfaces moving outward after break-off.

Parameters a and c may be determined for any pair of interfaces at a given time $t \leq 0$ (any pair of interfaces before break-off). These parameters determine the curvatures of the interfaces. In fitting the data to extract a and c, I have found that for my data it doesn't matter which image you use as long as it is near the time of break-off because the curvature is nearly constant as the interfaces approach. Specifically, given two separated interfaces as shown above in Fig. 16 I perform a second order polynomial fit of each interface and obtain two equations of the form $y = A_1 x^2 + B_1 x + C_1$ and $y = A_2 x^2 + B_2 x + C_2$. These equations may be simplified because the interfaces have been centered vertically so C_1 and C_2 are equal and opposite. Note this centering effectively removes the γ parameter from the theory as will be discussed after the fitting of a and c. Then by assuming the parabolas are symmetric across the y -axis, B_1 and B_2 are zero. These simplifications leave us with:

$$y = A_1 x^2 + const \quad (12)$$

$$y = A_2 x^2 - const \quad (13)$$

In this representation A_1 and A_2 denote the curvatures of the top and bottom interfaces respectively. In the theory parameters a and c determine interface curvatures in equation 10. Therefore by combining information from equations 10, 12 and 13 I can write a and c in terms of A_1 and A_2.

$$c = \frac{(A_1 + A_2)}{2} \quad (14)$$

$$a = \frac{(A_1 - A_2)}{2} \quad (15)$$

Namely c is the average of the two parabolic coefficients and a is half the difference of them. Also note that that equation 10 demands that these two parameters, a and c, have units of inverse length.

As I mentioned above the vertical centering that I performed effectively removes the γ parameter from the theory. This parameter is a "drift" parameter and accounts for any vertical shift of *both* interfaces in time. To explain my reasoning and application of this parameter I will direct the reader to Fig. 17 which describes two processes—one in accordance with the theory and one the physical reality of our experiment.

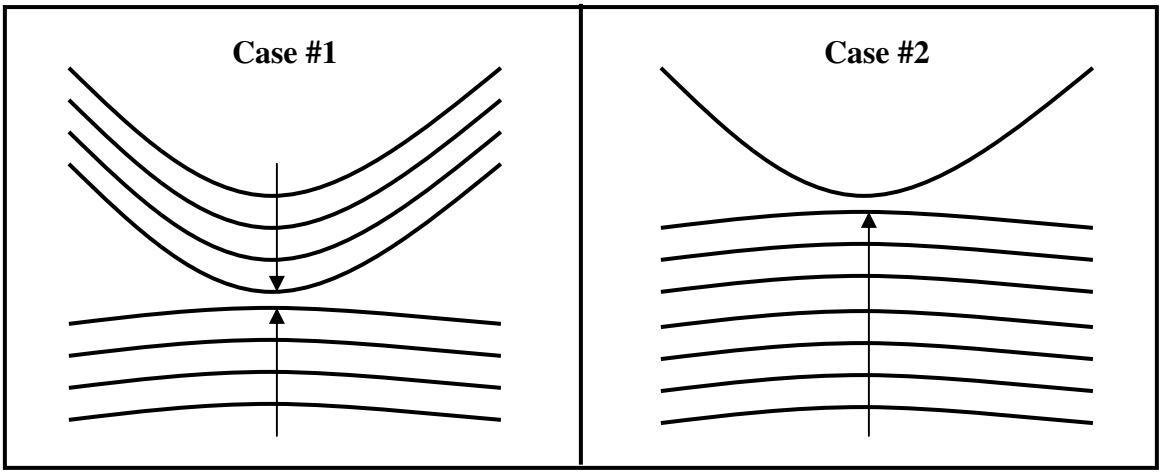

Figure 17: Each of these figures describes a possibility for interface motion. Case #1 on the left is what the theory expects in which both interfaces approach the point of break-off with the same constant speed. Case #2 on the right is the case I see experimentally in which the upper interface is stationary and the bottom interface approaches with a constant speed.

Our experimental interfaces move like those in case #2 in Fig. 17. In this case a drift parameter that tracks the concurrent movement of both interfaces cannot be directly applied because one of the interfaces is stationary. Instead, for each frame I center the two interfaces by calculating the vertex of each parabola and averaging these two points. I shift both interfaces so that this center point is $(0,0)$ which effectively shifts case #2 into case #1 and automatically makes any "drift" zero because this centering accounts for each interface moving at a different velocity as well as any shift in both interfaces.

I consider the centering I did to be a shift to the "center of break-off" frame. That is, the point $(0,0)$ always remains the point as which break-off will occur (assuming both interfaces approach it with equal and opposite velocity). The interfaces approach each other approximately constantly because oil is being pumped into a circle at a constant rate and the circle radius changes by less than 10% from the experiment's start to finish. Before break-off the centering is well defined. That is why I take the average of the two vertex points and shift that point to zero. On the other hand, after break-off occurs this process is no longer well defined because the vertices don't describe the drift or shift. In order to define the re-centering for after break-off I plotted the shift required to center vs. time for a series of images before break-off. This plot yields a linear relation and I made the assumption that it holds for after break-off to infer the correct centering distance. Equations 10 and 11 hold as written if I just redefine the drift parameter, γ, to be 1/2 the approach velocity of each interface and center the result. Note that to center the interfaces before break-off no additional information is needed, but to center them after break-off requires knowing how much each interface was shifted before break-off. I have effectively converted γ to zero in all plots, but γ remains present in calculations because it is needed to properly shift each pair of interfaces.

After a, c, and the drift, γ, are accounted for all that remains is the proper rescaling of time. In the theory time has units of length. Therefore the "proper rescaling" involves dividing time in units of area by a velocity to get time in units of seconds. The definition of the scaling velocity can be easily observed from equation 10 if you take $\gamma=0$ (for reasons explained above).

$$y=x^2(c\pm a)\pm t \quad (16)$$

Equation 16 clearly defines two parabolas with *y*-intercepts at $y=\pm t$. This means that the distance between the two interfaces is $2t$. Since I know the lab time, T, when this interface was collected I can scale time correctly under the assumption that the approach velocity is constant. Our results show that this assumption is correct up until the time of break-off. This means that any pair of extracted interfaces and the lab time at which the image was taken, T, relative to break-off lab time, $T_0=0$, is sufficient to calculate the proper scaling of time. The scaling velocity is one half the approach velocities of the two interfaces. Therefore the correct scaling velocity may generally be defined by the approach velocity as calculated from any two images from before break-off.

$$v_{scaling}=\frac{(T_1-T_2)}{2}(d_1-d_2) \quad (17)$$

A simpler case only calls for a single image (and use of the definition that the separation distance at $T=0$ is 0) to calculate the scaling velocity.

$$v_{scaling}=\frac{T_1}{2}d_1 \quad (18)$$

Where T_1 and d_1 are the lab time and interface separation distances respectively. Using this scaling equation (10) and (11) become the following in completely dimensional units.

$$y=x^2(c\pm a)\pm\frac{t}{v_{scaling}}+\frac{\gamma t}{v_{scaling}} \quad (19)$$

$$y=x^2\left(c\pm a\sqrt{1+\frac{2t}{ax^2v_{scaling}}}\right)+\frac{\gamma t}{v_{scaling}} \quad (20)$$

Results and Discussion

4.1 Comparison of Experimental Results to Theory

With a proper rescaling of time and fitting of parameters a and c, the next step is to plot the experiment and theory against each other. Below is a time sequence of these fittings assuming constant values for a, c, and γ throughout the process both before and after break-off. These images are plotted in units of pixels with a relation of 60 pixels/mm so these graphs fit a region about 2.7 mm (160 pixels) wide. The gray area is the theoretical oil domains and the white area is the theoretical air domains so the line separating the colors is the theoretical interface. The blue points plotted on the graph are the experimental interfaces extracted from images. The extent to which the blue points lay along the division between gray and white determines the theory's proficiency in predicting the time evolution of the process.

From the above fittings it is clear that the theoretical functions match the experiment nearly perfectly before break-off at lab time $T=0$. Then after this point the theory moves too fast compared to experiment for times after break-off.

4.2 Discussion

4.2.1 Theoretical Assumptions and Their Physical Realizations

A struggle between theoretical approximations and physical reality is prevalent throughout this work and so I will provide a discussion that details this interaction for each assumption. Lee *et al.* made a number of assumptions ranging from those that are commonly accepted to ones that severely constrain the break-off events applicable to this theory.

Figure 18: **(Next page)** This figure shows a comparison between the experimental and theoretical interfaces. The gray areas represent the theoretical oil domains and the white areas are the theoretical air domain therefore the red line marking the division between gray and white is the theoretical interface. Blue experimental interface points extracted from images of the interface, as described in section 3.3.1, are plotted on top of the theory. The extent to which the blue dots lay along the division between the gray and white areas determines how accurate the theory is. It is clear the theory is fairly accurate for $T \leq 0$, but for $T \geq 0$ the theory moves faster than the actual interface. Also note that the width of the experimental interface is due to the camera zoom. This distortion is due to the fact that at length scales on the order of the gap thickness the interface is curved and has a finite width. In these images this width is about 4-5 pixels wide which is about 50% of the gap thickness b

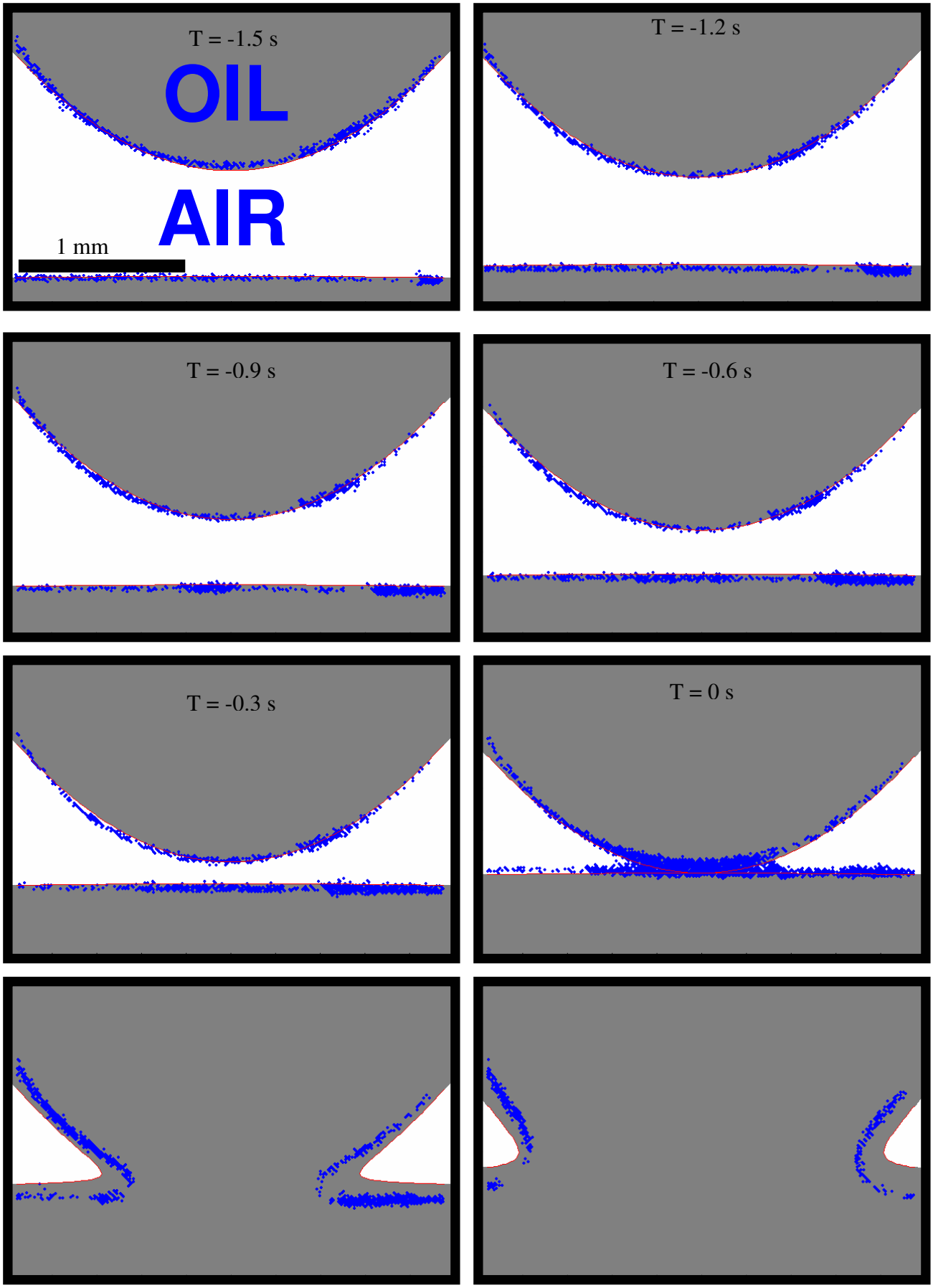
T = -1.5 s
OIL
AIR
1 mm
T = -1.2 s
T = -0.9 s
T = -0.6 s
T = -0.3 s
T = 0 s

The first assumption made is that both fluids are incompressible. Experimentally speaking the oil is almost certainly incompressible for any pressures that we look at and the air is approximately incompressible because the pressure is approximately a constant 1 atmosphere. A second assumption that the air has zero viscosity is also made. This is an acceptable approximation because the viscosity of air, $\mu_{air} = 1.8 \cdot 10^{-5}\, kg/m \cdot s$, compared to oil, $\mu_{oil} = 1 \cdot 10^{-3}\, kg/m \cdot s$, is much smaller.

The theory also assumes that the process is strictly two-dimensional. While this is certainly never the case experimentally but we attempt to approximate two-dimensions by making the third, z, dimension very small compared to the length scales of interest in the $xy-$plane. This assumption limits how close to break-off we can apply to theory because the bubble doesn't break-off until the interfaces are less than a gap thickness apart. Locally speaking bubble break-off is a three dimensional process because the gap thickness, z direction, is no longer small compared to dimensions in the $xy-$plane. Fig. 19 on the next page plots the interface separation in the $xy-$plane vs. time and the line $y = b$ to show when break-off becomes three dimensional. When break-off becomes three dimensional Lee's theory no longer applies according to their mathematics being strictly two dimensional.

The theory also makes the assumption that the bubbles maintain equal pressure after break-off. I ensure that by assuming that the air has zero viscosity and only looking at events in which the bubble is still connected after break-off occurs. This is why I look at a distorted annulus breaking off into a crescent shaped bubble. While this method produces a break-off event in which both bubbles maintain equal pressure there has been much discussion about whether the withdrawal of air is also required for the theory to hold. While the theory doesn't explicitly state that withdrawal of air is an assumption, Lee's suggested experiment (Fig. 4) does withdraw air. It is our hope that in an area local to the bubble the same conditions are met by a different mechanism which seems to be met because the interface moves at a constant velocity. In the case of our experiment in which an expanding annulus breaks off into a crescent shape the bubble area in a region ± ε from break-off along the axis of the neck the bubble area is decreasing because the annulus is becoming thinner as its radius is increased. In this manner we hope to have the same effect as removing air from the bubbles directly.

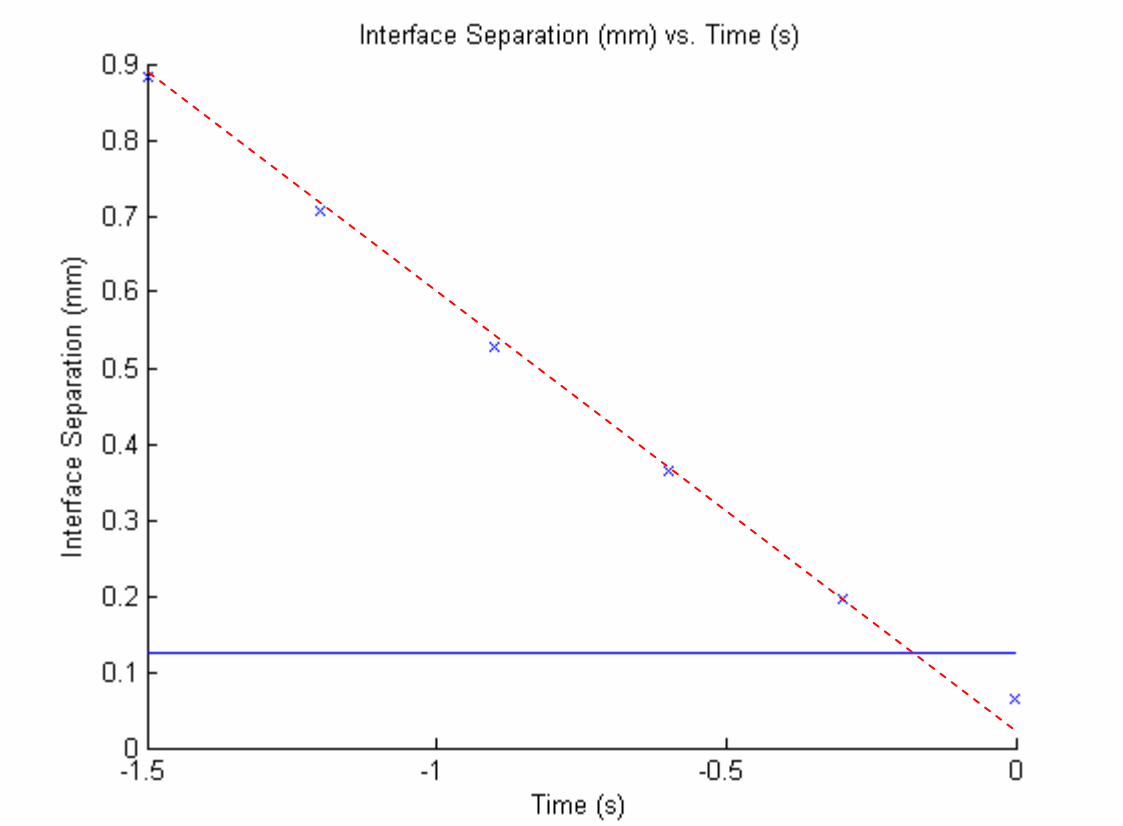

Figure 19: This plots the nearest distance (separation distance) of the two interfaces in the $xy-$plane leading up to break-off at $T=0$. At $T=-0.3$ the interface is only separated by approximately 1.5 times as thick as the gap so to the process becomes three dimensional and the Lee's theory is no longer applicable. The blue line is y = the gap thickness, b. Note that the separation distance calculated at $T=0$ isn't zero. This is because the interface has width and in the process of separating the interfaces the bottom of the top interface is put with the bottom interface so the fit used to calculate the separation is shifted upward slightly. The red dotted line shows that the interfaces approach each other with constant velocity. Figure 18 shows that at $T=0$ the interfaces are in contact with each other.

The final assumption and the most difficult is zero surface tension. In physical situations surface tension is never zero; in fact this assumption makes the capillary number, $Ca=\mu v/\sigma$, infinite. Having the non-dimensional parameter of interest for Hele-Shaw flows defined theoretically to be infinite is enough to make any experimentalist cringe, and the best that we can do it to make the capillary number as large as possible. In this experiment we kept the fluid and temperature the same so the dynamic viscosity μ, and surface tension σ are constant. Therefore to increase the capillary number we increase pumping rate in hopes of dominating the dynamics of the situation by the fluid flow and not surface tension.

4.2.2 How to Modify the Experiment

As stated in the above section there are considerable experimental barriers to accessing a regime in which Lee's theory is applicable. From the bubble break-off sequence presented in the section 4.1, it is apparent that the theory doesn't agree with the experiment after break-off. There are two directions we can go with this information—modify the theory to account for experimental parameters or modify the experimental conditions to comply better with the theory. Both of these are worthy endeavors and so I will address both.

According to my results from after break-off it appears like an additional term could be added to equation (20) to account for the discrepancy. The fits from T = 0.3 seconds and 0.6 seconds show theoretical and experimental interfaces which have roughly the same shape but the theoretical interfaces are shifted outward and slightly upward from the experimental ones. An additional term that translated the two post-break-off interfaces towards each other or one that slowed the rate at which the tips separated after break-off could effectively place the theory on top of experimental data. Such additional terms are purely a suggestion as to what would make the theory fit this situation better—I make no attempt to suggest the origin for deriving any such term explicitly.

In the regime of experiment I will make further, more accessible, suggestions as to how to obtain better results by more closely approximating the theory. First of all the fluid used could be changed to increase capillary number. If a more viscous fluid with smaller surface tension were used then the capillary number would be much larger and thus closer to a theory in which this number is infinite. Taking this idea one step further to increase capillary number miscible fluids could be used to make surface tension extremely small; this has the cost of a lot more work between experimental runs. While using an extremely viscous fluid increases capillary number I think that there is an ideal middle ground because as viscosity is increase the obtainable pumping rate is limited. If the fluid is too viscous then it isn't plausible, with the current syringe pump, to pump fast enough to make effects due to surface tension small.

Alterations of the gap in the Hele-Shaw cell could also move the experiment toward a regime in which the theory applied. Simply decreasing the gap thickness allows for areas closer to the point of pinch-off to be considered two-dimensional.

If further calculations show that it is required that air be withdrawn from the bubbles during the process of break-off then further research should be done to explore what determines where a bubble breaks off. If we had the ability to control where a bubble would break-off in the rectangular cell, which has two inlets, then we could perform the experiment as described in the theory. I think the next step should be to move the inlets closer to each other relative to the distance to the buffer. While I believe that the location of break-off is in nearly all cases *at* one of the two inlets, many times leaking to a buffer prevented me from even connecting the bubbles. It is possible that playing with this process more in a Hele-Shaw cell with two closely space inlets (relative to their distance from the buffer) could yield occasional break-off events that meet the theoretical conditions and experimental requirements for imaging may occur.

Beyond just moving the two inlets closer together, future research should examine modifying the cell to dictate where break-off occurs. In a qualitative sense from experience with these bubbles it seems like the bubbles break-off where it is most difficult to stay connected. In that sense I think that to make bubbles consistently break-off in the center of the cell away from the inlets the gap thickness can't be uniform—or likely even continuous. In a conventional Hele-Shaw cell that has a uniform gap thickness, identifying the point in the gap at which it is "most difficult to stay connected" undoubtedly leads to the inlets. One suggestion, purely a guess, is that making a Hele-Shaw cell in which half the gap is thicker than the other half might cause break-off to occur at this discontinuity in thickness instead of at an inlet. This change in gap thickness is not ideal, but the theory approaches the break-off problem in a mirror image case in which each side of the y-axis is symmetric so fitting each half of the interface separately may have a theoretical basis. It might be possible to obtain good data of half an interface breaking off at a position away from the inlet. Changing the gap thickness is just one suggestion. If modification of the gap is how future researchers want to approach the problem of controlling where break-off occurs then further thought should be put into what factors determine where a bubble will break-off.

Appendix A: Function Summaries

General Notes:

Plotter:

If "Plotter" is an input variable then if it is set to 1 the output for a given function will be displayed.

Point entry:

Several functions ask the user to enter points. This is done using the **getpts** function in Matlab. Points can be entered with the mouse by left clicking on the image. For the last point right mouse click to indicate that you are done entering points. NOTE: the right mouse click does get entered as a point.

X1, Y1, X2, Y2:

These variables will denote four arrays that contain the coordinates of points that constitute the interface for a given frame. In many instances a function will read in the two interfaces and return modified interfaces. In those cases the same variables will appear in the input and output variables and any changes will be explained in the function description.

Function: load

Call as [data{i}]=load(Filename.img, Plotter)

This function loads image given by the file name into the i^{th} element of the cell "data."

Function: section

Call as [X, Y]=section(image, Plotter)

Currently this function has all of the user entered data hard coded, but future modifications to improve the programs functionality are described below.

This function thresholds the given image using local averages. This function asks the user to enter pairs of points denoting the lower left and upper right corners of rectangular sections of the image. Then **section**() computes the average intensity value for the denoted rectangle and asks the user for a threshold value relative to the average intensity.

For data entry the function will loop in the following manner. First it asks for two points; left click the bottom left and right click the top right point. At any time you may stop entering rectangles by selecting only a single point—just right click the image to do

so. Once a rectangle is selected a gui interface will appear with a default threshold value equal to the average intensity. As you change the value in the gui interface the image will update the new threshold value. Click the appropriate button to increase this value until the interface looks correct and press done. Continue this process until the entire interface appears correctly.

This function returns two arrays containing the x and y coordinates of all points above the local threshold. It is important to note that **section()** reduces the image to a binary intensity distribution.

Functions: separate(), ck_separate(), mk_separate()

Separate:

Call as [points] = separate(image)

Separate() asks the user to select two points that indicate a straight line separating the two interfaces and returns these two points.

Ck_separate:

Call as [good]=ck_separate(image, points)

Ck_separate() displays the image and plots the line chosen in **separate()** and asks the user to select 2 points if it's correct and 1 otherwise.

Mk_separate

Call as [X1,Y1,X2,Y2] = mk_separate(image, X,Y,points,Plotter)

Input variables, image, x and y coordinates denoting the threshold values, the points from **separate()** and plotter. Output is two sets of x-y coordinates denoting the two separated interfaces.

Functions: angle_mark(), find_angle(), and rotate_data()

Angle_mark:

Call as [mark_x,mark_y]=angle_mark(image)

This function just displays the current image and lets the user mark points on the image so that the proper rotation can be found. These points are then returned so that they can be displayed in the **find_angle()** function.

Find_angle:

Call as [angle] = find_angle(X1,Y1,X2,Y2,mark_x,mark_y, step, start)+3.14159

X1, Y1, X2, Y2: two sets of coordinate pair arrays denoting the two interfaces.

Mark_x, mark_y: x-y coordinates for the points to help recognize the correct orientation—these are created using the **angle_mark()** function.

Step: Angle increment.

Start: Start angle.

To select the correct angle right click on the image until it is oriented corrected then select two points to quit the function. (Note: selecting 2 points is the only way to exit, selecting 1 or >2 points will just increment the rotation once more.)

Rotate:

Call as [rX,rY]=rotate(X,Y,angle)

This function rotates the given interface coordinates X and Y by "angle" radians and returns the new interface.

Functions: find_center, crop_data, find_center2, and center

Find_center

Call as [X1,Y1,X2,Y2,c_x,c_y]=find_center(X1,Y1,X2,Y2)

This function asks the user to click on the center (point of break-off) and then returns the images centered at that point. X1, Y1, X2, and Y2 are the coordinates for the two separated interfaces and cX1, cY1, cX2, cY2 are the centered interfaces.

Find_crop

Call as [X1,Y1,X2,Y2,l_x,b_y,t_y] = find_crop (X1,Y1,X2,Y2,Plotter)

This function reads in a centered interface and outputs a cropped interface. To crop the interface down to a region "near" break-off this function asks the user to select one point to indicate x-lower and y-lower and another point to indicate y-upper. The user should select the lower left and upper right points of a rectangle enclosing the intended window. The final result is that all points outside of the rectangle defined by (l_x,b_y) and (-l_x, t_y) are removed from the interface coordinate arrays and the new interfaces and window bounds are returned so that further interfaces may be cropped to the same window without needing user input.

Find_center2:

Call as [X1,Y1,X2,Y2,c2_x,c2_y]=find_center2 (X1,Y1,X2,Y2)

This function centers the data by performing second order polynomial fits to both interfaces and calculates the minima (or maxima of the bottom parabola) and averages

the two x-y points to find the minimum. The data is then shifted to this center and returned by the function. The center-x, c2_x, and center-y, c2_y, values are also returned so that further images can be shifted to the same center. NOTE: to properly shift raw images one must shift them to (c_x+c2_x, c_y+c2_y) where (c_x, c_y) is the center obtained from **find_center()** and (c2_x, c2_y) is the center returned from **find_center2()**.

Center:

Call as [X1, Y1, X2, Y2]=center(X1, Y1, X2, Y2, c_x, c_y)

This function reads in the two interfaces and the value for the correct center. This center value should be the sum of the two values, which were manually found for the first image using **find_center()** and computed in **find_center2()**. The returned interface is centered on the same point as the first image so that drift may be observed, however eventually I removed this function because the drift parameter could not correctly account for the drift experienced in out experiment.

Functions: calc_const and theory

Calc_const:

Call as [a,c,g]= calc_const(X1, Y1, X2, Y2)

This function calculates and returns the three parameters necessary to specify the theoretical interface given by Lee *et al.* for the given frame/interfaces.

Theory:

Call as [TX, TY1, TY2] = theory(X1, Y1, X2, Y2, l_x, frame_number, t_end, t_step, a, c, g, Plotter)

This function returns the theoretical interfaces at a time specified by the frame number. If Plotter is one then a plot of the experimental and theoretical interfaces will be displayed.

Bibliography

[1] S-Y. Lee, E. Bettelheim, and P. Wiegmann. Bubble break-off in Hele-Shaw flows—singularities and integrable structures. *Physica D* **219**:22-34, 2006.

[2] H.S. Hele-Shaw. The Flow of Water. *Nature* **58**:34–36. 1898.

[3] D. J. Tritton. Physical Fluid Dynamics: Second Edition. Oxford University Press. Walton Street, Oxford. 1988.

[4] J.C. Burton, R. Waldrep, and P. Taborek. Scaling and Instabilities in Bubble Pinch-Off. *Physical Review Letters* **94**:184502, 2005.

[5] R. Ishiguro, F. Graner, E. Rolley, and S. Balibar. Coalescence of Crystalline Drops. *Physical Review Letters* **93**:235301, 2004.

[6] R. Bergmann, D. Meer, M. Stijnman, M. Sandtke, A. Prosperetti, and D. Lohse. Giant Bubble Pinch-Off. *Physical Review Letters* **96**:154505, 2006.

[7] I. Cohen, M. Brenner, J. Eggers, and S. Nagel. Two Fluid Drop Snap-Off Problem: Experiment and Theory. *Physical Review Letters* **83**(6):1147-1150, 1999.

[8] W. Zhang and J. Lister. Similarity Solutions for Capillary Pinch-Off in Fluids of Differing Viscosity. *Physical Review Letters* **83**(6):1151-1154, 1999.

[9] T. Maxworthy. Bubble formation, motion and interaction in a Hele-Shaw cell. *Journal of Fluid Mechanics* **173**:95-114, 1986.

[10] M. G. Moore, A. Juel, J. M. Burgess, W. D. McCormick, and H. L. Swinney. Fluctuations and pinch-offs observed in viscous fingering. *Proceedings of the Seventh Experimental Chaos Conference.* (**676**)189-194. 2003.

M. G. Moore, A. Juel, J. M. Burgess, W. D. McCormick, and H. L. Swinney. Fluctuations in Viscous fingering. *Physical Review E* **65**:030601. 2002.

[11] P.G. Saffman and G. Taylor. The penetration of a fluid into a porous medium or Hele-Shaw cell containing a more viscous liquid. *Proceedings of the Royal Society of London. Series A, Mathematical and Physical Sciences* **45**(1242):312-329, 1958.

[12] M. Mineev-Weinstein. Selection of the Saffman-Taylor Finger Width in the Absence of Surface Tension: An Exact Result. *Physical Review Letters* **81**(10):2113-2116, 1998.

[13] L. Ristroph, M. Thrasher, M. Mineev-Weinstein, and H. Swinney. Fjords in viscous fingering: Selection of width and opening angle. *Physical Review* **74**:015201(R), 2006.

[14] M. G. Moore. *Unsteady Growth and Relaxation of Viscous Fingering*. PhD Dissertation. The University of Texas at Austin. 2003.

[15] E. Lajeunesse and Y. Couder. On the tip-splitting instability of viscous fingering. *Journal of Fluid Mechanics* **413**:125-149, 2000.